Infinite dipolar droplet: A simple theory for the macrodroplet regime

Sukla Pal ◐, D. Baillie ◐, and P. B. Blakie ◐

Department of Physics, Centre for Quantum Science, and The Dodd-Walls Centre for Photonic and Quantum Technologies,
University of Otago, Dunedin 9016, New Zealand

In this paper we develop a theory for an infinitely long droplet state of a zero-temperature dipolar bosonic gas. The infinite droplet theory yields simpler equations to solve for the droplet state and its collective excitations. We explore the behavior of infinite droplets using numerical and variational solutions, and we demonstrate that it can provide a quantitative description of large finite droplets of the type produced in experiments. We also consider the axial speed of sound and the thermodynamic limit of a dipolar droplet.

I. INTRODUCTION

Dipolar bosonic gases of magnetic atoms interact with a long-ranged and anisotropic dipole-dipole interaction (DDI). Experiments using the highly magnetic atoms of dysprosium [1–3] and erbium [4] have prepared one or several self-bound quantum droplets that cohere, even in the absence of any external confinement (see also subsequent nondipolar droplets [5,6]). These quantum droplets occur in the dipole-dominated regime, where the short-ranged s-wave interactions are weaker than the DDIs [7,8] and the overall two-body interactions are attractive. In this regime the effects of quantum fluctuation corrections become important [9–11] and stabilize the droplets against mechanical collapse [12–15]. An important effect of the DDIs is that the droplets take a filament shape—elongating in the direction that the dipoles are polarized—to minimize the DDI energy. Due to the long-ranged and anisotropic character of the DDI and the highly elongated droplet shape, quantitative calculations for the droplet states and their excitations are a challenging numerical problem.

Here we develop an infinite droplet theory. In this theory we consider the idealized case of a droplet that is an infinitely long filament (along the direction of the dipole orientation) of specified linear density n (see Fig. 1). This idealization should be a good approximation to a finite droplet with sufficiently many atoms N that it is highly elongated. Such droplets, often referred to as macrodroplets, have been prepared with $N \sim 2 \times 10^4$ atoms [4] and can persist as self-bound droplets even in the absence of any confinement [3].

We present results for the infinite droplet using numerical solutions and a variational approximation we develop. We explore the character of the infinite droplet excitations and show that the recently identified "antiroton" effect [16] plays an important role in the spectrum of a droplet. We consider a mapping to compare the infinite droplet results to a finite droplet, and we use this to make a comparison to the excitation spectrum of a finite droplet. We find that often the infinite droplet is not mechanically stable, with long wavelength axial modes being dynamically unstable. In these cases the axial speed of sound of the infinite droplet is imaginary. However, as these instabilities only manifest at wavelengths that are much longer than the length of the finite droplet, they can be considered inconsequential, and the corresponding finite droplet is stable. Finally, we consider taking a finite droplet to the thermodynamic limit by letting $N \to \infty$, which is different than the infinite dipolar droplet.

II. FORMALISM

A. EGPE theory

It is now well-established (e.g., see Refs. [2–4,7,8,14,15][1]) that the coherent atomic field $\psi(\mathbf{r}) = \langle \hat{\psi}(\mathbf{r}) \rangle$ of a quantum droplet is governed by the extended Gross-Pitaevskii equation (EGPE) that includes the effects of beyond-mean-field quantum fluctuations. The EGPE takes the form $\mathcal{L}\psi = \mu\psi$, where μ is the chemical potential and

$$\mathcal{L} \equiv -\frac{\hbar^2 \nabla^2}{2M} + V_{\mathrm{tr}} + \int d\mathbf{r}' U(\mathbf{r} - \mathbf{r}')|\psi(\mathbf{r}')|^2 + \gamma_{\mathrm{QF}}|\psi|^3, \tag{1}$$

$$V_{\mathrm{tr}} = \tfrac{1}{2}M\omega_\rho^2(x^2 + y^2) \tag{2}$$

are the EGPE operator and trapping potential, respectively, with M being the mass of the atom. Here only transversal harmonic confinement is considered with the angular frequency ω_ρ, although many of our results are for the free-space case of $\omega_\rho = 0$. The two-body interactions are described by the interaction potential

$$U(\mathbf{r}) = g_s\delta(\mathbf{r}) + \frac{3g_{\mathrm{dd}}}{4\pi r^3}\left(1 - \frac{3z^2}{r^2}\right). \tag{3}$$

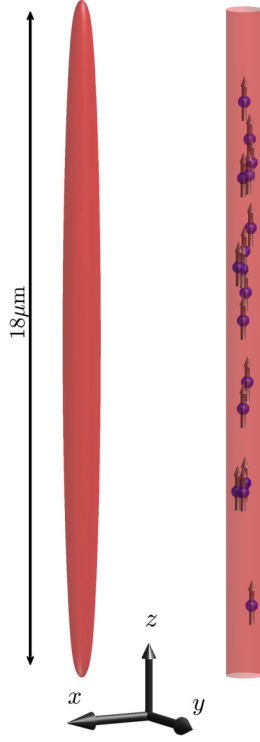[1]Alternative theories to the EGPE have been developed, e.g., see Refs. [17,18].

FIG. 1. (Left) Density isosurface of a finite free-space droplet with $N = 2.5 \times 10^4$ ^{164}Dy atoms, $a_{\rm dd} = 130.8a_0$, and $a_s = 80a_0$. (Right) Schematic of a section of the infinite dipolar droplet we develop here.

Here $g_s = 4\pi a_s \hbar^2 / M$ is the short-ranged coupling constant, where a_s is the s-wave scattering length. The atoms have magnetic dipoles of moment μ_m aligned along the z axis by an external bias field. The DDIs between the atoms are characterized by the coupling constant $g_{\rm dd} = 4\pi \hbar^2 a_{\rm dd} / M$, where $a_{\rm dd} = \mu_0 \mu_m^2 M / 12\pi \hbar^2$. The quantum fluctuations are described by the higher-order local nonlinear term with the coefficient (see Refs. [10,11,15])

$$\gamma_{\rm QF} = \frac{32}{3} g_s \sqrt{\frac{a_s^3}{\pi}} \left(1 + \frac{3}{2} \epsilon_{\rm dd}^2 \right), \tag{4}$$

where $\epsilon_{\rm dd} = a_{\rm dd} / a_s$.

B. Infinite droplet state

Here we develop a model for a droplet that is infinitely long and translationally invariant along the z axis, i.e.,

$$\psi(\mathbf{r}) = \sqrt{n} \chi(\rho), \tag{5}$$

where n is the specified linear density and $\chi(\rho)$ is the unit normalized transverse mode. Here we have utilized cylindrical symmetry to reduce the dependence of the transverse mode to the radial coordinate $\rho = \sqrt{x^2 + y^2}$. A decomposition similar to Eq. (5) was explored previously in Ref. [16] (also see Ref. [19]) as a model of a dipolar condensate in an elongated tube trap. Here we extend this theory to include quantum fluctuations and hence the droplet regime which occurs when the DDI interactions dominate over the contact interactions (i.e., $\epsilon_{\rm dd} > 1$). In this regime the droplet can exist (as a transversally

localized state) even in the absence of any transverse confinement, i.e., can become self-bound. Using (5), the EGPE simplifies to

$$\mathcal{L}^\perp \chi = \mu \chi, \tag{6}$$

where

$$\mathcal{L}^\perp \equiv -\frac{\hbar^2}{2M\rho} \frac{\partial}{\partial \rho} \left(\rho \frac{\partial}{\partial \rho} \right) + V_{\rm tr} + n(g_s - g_{\rm dd}) |\chi(\rho)|^2 \\ + n^{3/2} \gamma_{\rm QF} |\chi(\rho)|^3. \tag{7}$$

Notice that for the infinite droplet state the two-body interactions appear as an effective contact interaction. We can see this from the k space form of the interaction potential, (i.e., the Fourier transform of Eq. (3), see Ref. [20])

$$\tilde{U}(\mathbf{k}) = g_s + g_{\rm dd} \left(\frac{3k_z^2}{k^2} - 1 \right), \tag{8}$$

which approaches the constant value $g_s - g_{\rm dd}$ in the $k_z \to 0$ limit appropriate to the infinite droplet state.

Because Eq. (7) does not involve an explicit long-range interaction term, it avoids many of the technical issues that normally arise in solving the EGPE with DDIs. Thus, the transverse profile of the infinite droplet state can be solved for using standard packages for solving the Gross-Pitaevskii equation adapted to include the higher-order local nonlinearity of the quantum fluctuation term.

C. Excitations of the infinite droplet

Bogoliubov theory provides a description of the quasiparticle excitations of the droplet [12,21]. These excitations can be obtained by linearizing the time-dependent GPE, $i\hbar \partial_t \psi = \mathcal{L}\psi$, about the stationary state, $\sqrt{n}\chi$, using the ansatz

$$\psi(\mathbf{r}, t) = e^{-i\mu t} \left\{ \sqrt{n}\chi(\rho) + \sum_{k_z, m, j} \left[c_{k_z m j} u_{k_z m j}(\rho) e^{im\phi + ik_z z - iE_{k_z m j} t/\hbar} \right. \right. \\ \left. \left. - c_{k_z m j}^* v_{k_z m j}^*(\rho) e^{-im\phi - ik_z z + iE_{k_z m j}^* t/\hbar} \right] \right\}, \tag{9}$$

where ϕ is the azimuthal angle. Here $\{u_{k_z m j}, v_{k_z m j}\}$ are the quasiparticle modes with respective eigenvalues $\{E_{k_z m j}\}$, and $\{c_{k_z m j}\}$ are (small) c-number amplitudes. The z components of linear and angular momentum of the quasiparticle are given by $\hbar k_z$ and $\hbar m$, respectively, and the quantum number j characterizes the transverse (vibrational) mode. The quasiparticles are obtained by solving the Bogoliubov–de Gennes (BdG) equations

$$E_{k_z m j} \begin{pmatrix} u_{k_z m j} \\ v_{k_z m j} \end{pmatrix} = \begin{pmatrix} \mathcal{L}_{k_z m} - \mu & -X_{k_z m} \\ X_{k_z m} & -(\mathcal{L}_{k_z m} - \mu) \end{pmatrix} \begin{pmatrix} u_{k_z m j} \\ v_{k_z m j} \end{pmatrix}, \tag{10}$$

where $\mathcal{L}_{k_z m} \equiv \mathcal{L}^\perp + \epsilon_{k_z} - \frac{\hbar^2 m^2}{2M\rho^2} + X_{k_z m}$, $\epsilon_{k_z} = \frac{\hbar^2 k_z^2}{2M}$ is the free-particle dispersion relation, and the exchange term is

$$X_{k_z m} f \equiv n\chi e^{im\phi} \mathcal{F}^{-1} \{ \tilde{U}(\mathbf{k}_\rho + k_z \hat{\mathbf{z}}) \mathcal{F}\{\chi f e^{-im\phi}\} \} \\ + \frac{3}{2} \gamma_{\rm QF} n^{3/2} |\chi|^3 f, \tag{11}$$

with $\mathcal{F}$ denoting the planar Fourier transform in $\boldsymbol{\rho} = (x, y)$, and $\mathbf{k}_\rho = (k_x, k_y, 0)$ being the reciprocal space vector. The

excitations explicitly depend on the k-space interaction potential, and care needs to taken to deal with finite grid size effects in numerical calculations (e.g., using a cutoff interaction, see Refs. [22–24]).

D. Variational theory

A variational approach can also be used to develop an approximate description of the infinite droplet. Here we approximate the transverse mode by a radially symmetric Gaussian,

$$\chi^{\text{var}}(\rho) = \frac{e^{-\rho^2/2l^2}}{\sqrt{\pi}l}, \tag{12}$$

where the width l is considered as a variational parameter. The energy density per particle of the variational state is (from Ref. [16], but extended to include the quantum fluctuation term)

$$\mathcal{E} = \frac{\hbar^2}{2Ml^2} + \frac{M\omega_\rho^2 l^2}{2} + \frac{n(g_s - g_{\text{dd}})}{4\pi l^2} + \frac{4n^{3/2}\gamma_{\text{QF}}}{25\pi^{3/2}l^3}. \tag{13}$$

The variational solution is determined by minimizing Eq. (13) with respect to l.

The lowest ($m = 0$, $j = 0$) band of excitations can be obtained from the variational theory under the same shape approximation [16] (also see Ref. [19]), i.e., setting $u_{k_z 00}$ and $v_{k_z 00}$ to be proportional to χ^{var}. This yields the dispersion relation (also see Ref. [25])

$$E_{k_z}^{\text{var}} = \sqrt{\epsilon_{k_z}\left[\epsilon_{k_z} + 2n\tilde{U}_0(k_z) + 3n^{3/2}\gamma_{\text{QF}}\gamma_\chi\right]}, \tag{14}$$

where $\gamma_\chi \equiv \frac{2}{5\pi^{3/2}l^3}$, and

$$\tilde{U}_0(k_z) = \frac{g_s - g_{\text{dd}}}{2\pi l^2} - \frac{3g_{\text{dd}}}{2\pi l^2}Q^2 e^{Q^2}\text{Ei}(-Q^2), \tag{15}$$

with $Q^2 \equiv k_z^2 l^2/2$ and Ei being the exponential integral.

The behavior of the effective interaction $\tilde{U}_0(k_z)$ that appears in the variational theory is shown in Fig. 2 for a system in the droplet regime, where $g_{\text{dd}} > g_s$. This emphasizes the limiting values of $\tilde{U}_0(k_z)$, notably $\lim_{k_z \to 0} \tilde{U}_0 = (g_s - g_{\text{dd}})/2\pi l^2$ and $\lim_{k_z \to \infty} \tilde{U}_0 = (g_s + 2g_{\text{dd}})/2\pi l^2$. In the droplet regime these limits are attractive and repulsive, respectively. We note that a comparison of $\tilde{U}_0(k_z)$ to the effective interaction obtained using a numerical solution of the GPE is presented in Fig. 2 of Ref. [16], showing that the variational approach provides a good approximation.

III. RESULTS

A. Dynamic structure factor of an infinite droplet

The zero-temperature dynamic structure factor within the Bogoliubov theory is given by

$$S(k_z, \omega) = \sum_j |\delta n_{k_z j}|^2 \delta(\omega - E_{k_z 0 j}/\hbar), \tag{16}$$

where $\delta n_{k_z j} = \int d\rho\, 2\pi\rho[u_{k_z 0 j}^*(\rho) - v_{k_z 0 j}^*(\rho)]\chi(\rho)$. Here we have considered the dynamic structure factor for a wave vector along z and in this case only the $m = 0$ excitations contribute. The dynamic structure factor characterizes the structure of the system and its collective excitations. In cold-gas experiments
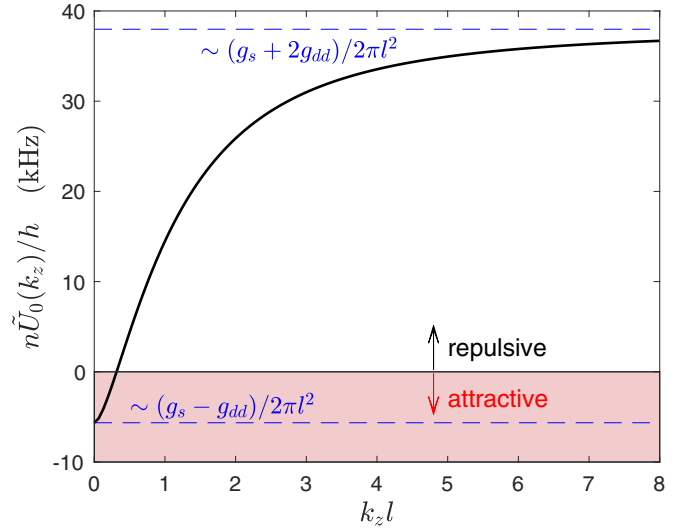

FIG. 2. Variational theory effective interaction $\tilde{U}_0(k_z)$ with the low-k_z and high-k_z limits shown. Results for a ^{164}Dy system with $n = 2.5 \times 10^3/\mu\text{m}$, $a_s = 80a_0$, $a_{\text{dd}} = 130.8a_0$, and $l = 0.383\,\mu\text{m}$.

the zero-temperature dynamic structure factor can be measured by Bragg spectroscopy (e.g., see Refs. [26–28]), and this technique has been applied to dipolar condensates in the roton [29] and the supersolid [30] regimes.

In Figs. 3(a)–3(c) we show the dynamic structure factor for free-space droplets with various values of a_s. As a_s decreases (ϵ_{dd} increases) the droplet is more tightly bound, as revealed by the chemical potential becoming more negative. The BdG energies are measured relative to the chemical potential, and the excitations with $E_{k_z m j} < -\mu$ are below threshold and are thus bound to the droplet. Our results show that only one of the $m = 0$ branches is bound and it joins up with a continuum of transverse excitations when $E_{k_z 00} > \epsilon_{k_z}^{\text{cont}} \equiv -\mu + \epsilon_{k_z}$. The bound excitation branch is only apparent in Figs. 3(b) and 3(c) where μ is sufficiently negative.

In Figs. 3(d)–3(f) we consider cases with the same parameters used for Figs. 3(a)–3(c), but with the addition of transverse confinement. For the highest value of scattering length [Fig. 3(d)] the chemical potential is positive and the system cannot be considered as a *self-bound* droplet. The observed behavior in this regime is similar to previous work considering a dipolar condensate in an elongated trap (e.g., see Fig. 3 of Ref. [16][2]). A noticeable effect of the transverse confinement is that discrete excitation bands remain at all energy scales (i.e., there is no continuum of transverse excitations). These results also exhibit features that were collectively referred to as the "antiroton" effect in Ref. [16]. That work considered a dipolar condensate in an elongated trap with the dipoles polarized along the long axis of the trap. The features of this effect were identified as (i) a rapidly rising, and upward curving, lowest excitation band and (ii) the emergence of a strong multiband response at high k_z. These features arise

---

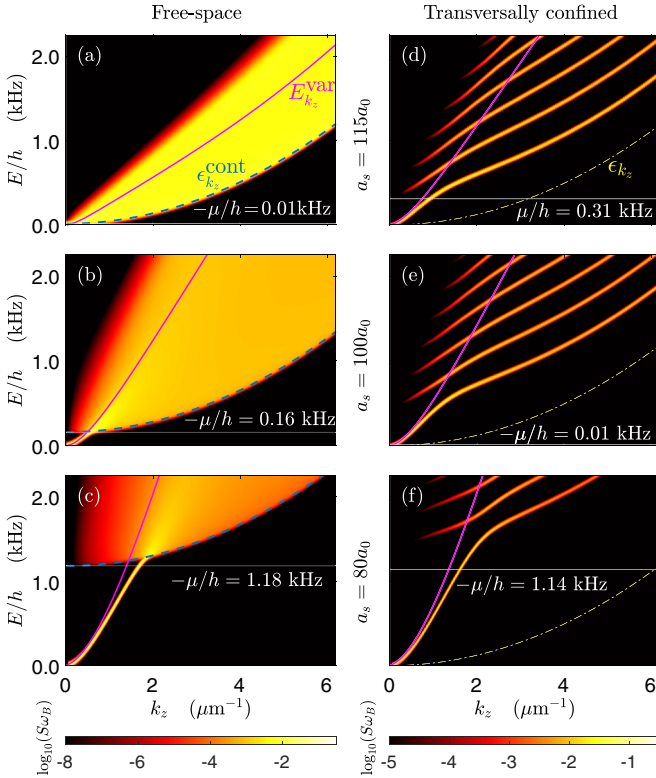[2]We note that because Ref. [16] did not include quantum fluctuations it was restricted to the regime $a_s > a_{\text{dd}}$.

FIG. 3. (a)–(c) The dynamic structure factor $S(k_z, \omega)$ for an infinite droplet state of ^{164}Dy atoms with $n = 2.5 \times 10^3/\mu m$ and for (a,d) $a_s = 115a_0$, (b,e) $a_s = 100a_0$, and (c,f) $a_s = 80a_0$. Cases (a)–(c) are in free-space ($\omega_\rho = 0$) and cases (d)–(f) are confined with $\omega_\rho/2\pi = 150$ Hz. The variational result for $E_{k_z}^{\text{var}}$ is shown with magenta solid lines. The lower bound of the continuum $\epsilon_{k_z}^{\text{cont}}$ is shown by the blue dashed lines in panels (a)–(c), and in panels (d)–(f) the yellow dash-dot line shows the free-particle dispersion ϵ_{k_z}. We broadened the δ function in the dynamic structure factors by setting $\delta(\omega) = e^{-(\omega/\omega_B)^2}/\sqrt{\pi}\omega_B$, with $\omega_B/2\pi = 15$ Hz.

from the interactions becoming increasingly repulsive[3] with increasing k_z. This situation arises in the droplet where the $k_z \to 0$ interaction is attractive, allowing the droplet to bind tightly, while as k_z increases the interaction becomes strongly repulsive (e.g., see Fig. 2). This causes a strong interaction between the respective excitations and the droplet and is the origin of the multiband response. In the multiband regime the transverse profile of the lowest band of excitations changes shape to reduce overlap (and hence interaction) with droplet. For k_z values where this reshaping occurs [e.g., $k_z \sim 1/\mu m$ in Figs. 3(d)–3(f)], the structure factor response weight [i.e., $\delta n_{k_z j}$] is transferred to higher excitation bands. The variational approach for the lowest excitation band assumes these modes to have the same transverse shape as the droplet and thus fails to capture the multiband response. We also observe that aspects of the antiroton effect carry over to the free-space droplet. First, the ground band curves up rapidly. Second, the multiband behavior becomes a region of stronger response in the continuum of excitations [see Figs. 3(b) and 3(c)].

We note that in all free-space results [Figs. 3(a)–3(c)] and the most strongly bound trap case [Fig. 3(f)] that the lowest excitation band $E_{k_z 00}$ is imaginary for very small k_z values [e.g., Im$\{E_{k_z 00}\}$ for the case in Fig. 3(c) is shown in the lower inset to Fig. 6(a)]. We neglect the weight of these modes in Fig. 3 and return to discuss them further in Sec. III C.

B. Excitation spectrum of a finite droplet

We now consider how to apply the infinite droplet theory to characterize the excitation spectrum of a finite droplet. A finite droplet configuration is specified by the parameters $\{a_s, a_{\text{dd}}, N\}$. Here we take the corresponding infinite droplet to have a linear density identified with the linear density at the center ($z = 0$) of the finite droplet, i.e.,

$$ n = \int d\boldsymbol{\rho} |\psi(\boldsymbol{\rho}, 0)|^2, \tag{17} $$

where $\psi(\boldsymbol{\rho}, z)$ is the wave function of the finite droplet. In Figs. 4(a)–4(c) we compare aspects of the transverse density profiles obtained using this mapping. Figure 4(e) shows the linear density as a function of N obtained from finite droplet calculations according to Eq. (17). This linear density is the only additional input into the infinite droplet theory.

These results show that the infinite droplet generally provides a good description of the radial profile except for low-atom-number cases close to where the droplet unbinds [see Figs. 4(a) and 4(c)]. This coincides with the finite droplet having its smallest aspect ratio [Fig. 4(d)], where the approximation of the droplet being infinite is least appropriate. While the infinite droplet theory is seen to work very well for large N (i.e., the macrodroplet regime), the variational description works less well in this regime. This is because the density of the droplet saturates towards a maximum value,[4] causing the transverse density profile to develop a flat top that is not well-described by a Gaussian.

Using our mapping we can provide an approximate description of the excitation spectrum of a finite droplet. Here we compare to results presented in Ref. [21] for the spectrum of a finite droplet, obtained using large-scale diagonalization procedures. Some results of that work are reproduced in Fig. 5. In this regime the droplet is highly elongated ($\sigma_z/\sigma_\rho \approx 30$) and acts as a waveguide for the low-energy collective modes. The excitations appear as a set of bands labeled by their z component of angular momentum.[5] In Ref. [21] an approximate dispersion relation, equivalent to our variational result (14), was used to provide a qualitative description of the $E_{k_z 00}$ band. This variational result does not describe any of the higher bands (see Fig. 5). In contrast the infinite droplet theory [numerically solving Eqs. (10)] exhibits good quantitative agreement with the finite droplet results for the $m = 0$, 1, and 2 bands of excitations presented in Ref. [21]. We also show the

---

[3]cf. the roton effect where the interactions are attractive at high k_z.

---

[4]The maximum value arises from the balance of the attractive two-body interactions and the repulsive quantum fluctuations.

[5]In a finite droplet, the z component of momentum is not a good quantum number and in Ref. [21] an approximate mapping was developed by analyzing the approximate wavelengths of the individual excitations.
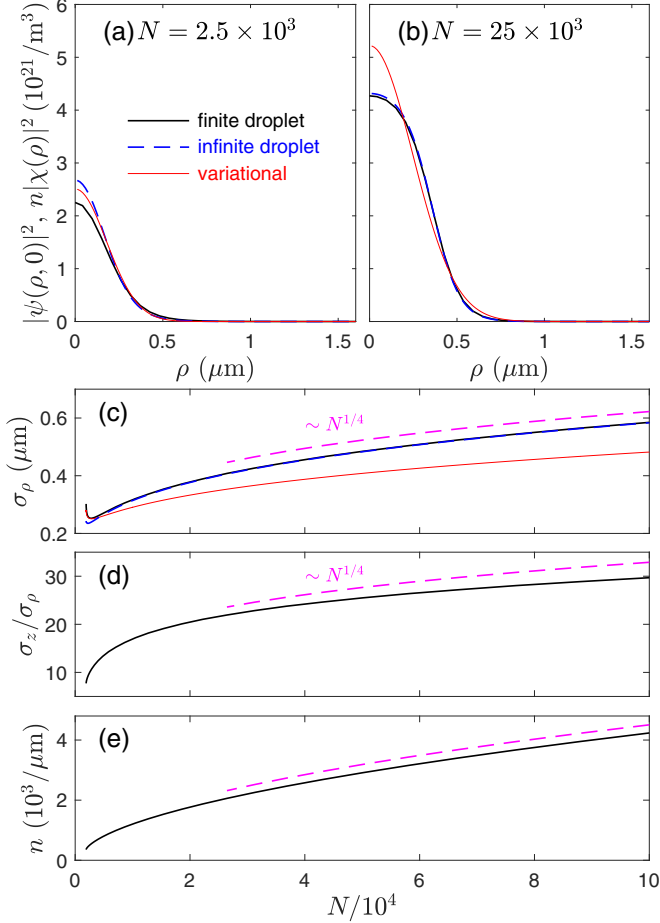
FIG. 4. Mapping and comparison of finite and infinite droplets. The $z = 0$ transverse density profile for a finite droplet with (a) $N = 2.5 \times 10^3$ and (b) $N = 25 \times 10^3$ atoms compared to the infinite droplet results. (c) Comparison of the $1/e$-density half-width σ_ρ in the $z = 0$ plane as the number of atoms in the droplet varies (for the variational theory this is l). The finite droplet (d) aspect ratio and (e) linear density (17) as N varies. Here σ_z is the $1/e$-density half-width of the droplet on the z axis. These results are for a free-space droplet of ^{164}Dy atoms with $a_{\text{dd}} = 130.8a_0$ and $a_s = 80a_0$. The droplet is only self-bound for N exceeding the critical value of $N_c \approx 1899$.

infinite droplet predictions for the $m = 3$ band (not calculated in Ref. [21]), with the higher angular momentum bands lying in the continuum (see the inset to Fig. 5). We note that the finite droplet theory predicts that the $E_{k_z 00}$ band is imaginary in the small-k_z limit (well below where the first excitation occurs in the finite droplet).

C. Axial speed of sound and long-wavelength instability of the infinite droplet

The excitation spectrum of a dipolar condensate is known to be anisotropic (e.g., see Refs. [31–35]) due to the anisotropy of the DDIs. Here we explore the axial speed of sound of a dipolar droplet—i.e., the speed of sound along the long axis of the droplet. We identify the axial speed of sound from the long-wavelength slope of the lowest excitation
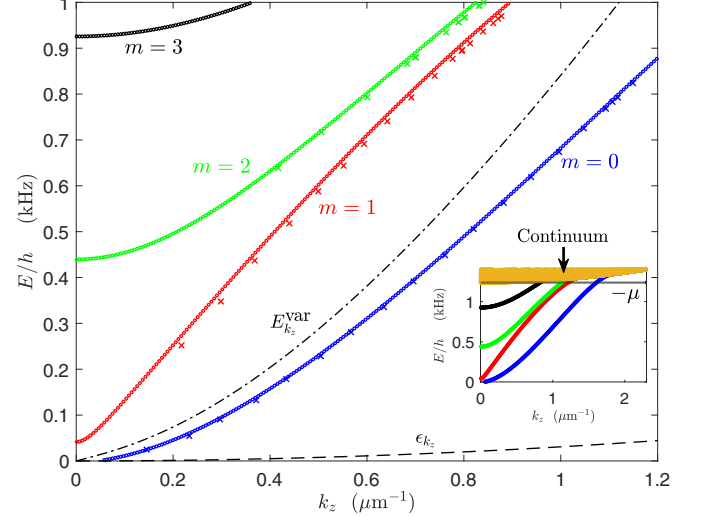

FIG. 5. Excitation spectrum of a free-space droplet of $N = 10^5$ ^{164}Dy atoms with $a_s = 80a_0$. The BdG excitation energies of a finite droplet are plotted as $\times$ symbols against a z-wave-vector assignment (these results are from Ref. [21] and assignment details are discussed therein). Results are sorted by the z component of angular momentum of the excitation [blue ($m = 0$), red ($m = 1$), green ($m = 2$), and black ($m = 3$)]. Solid lines give the infinite droplet results for comparison using the linear density $n = 4231.6/\mu$m. Black dash-dotted lines give the variational result, Eq. (14), and the black dashed line shows ϵ_{k_z} for reference. The inset shows the infinite droplet result including the continuum excitations that develop at higher energies. Note that the $E_{k_z 00}$ band (blue dots) becomes imaginary for $k_z \lesssim 0.04\ \mu$m^{-1}.

band as

$$c_z = \frac{1}{\hbar} \left. \frac{\partial E_{k_z 00}}{\partial k_z} \right|_{k_z = 0}. \tag{18}$$

The $E_{k_z 00}$ excitation band was observed in Figs. 3 and 5 to have novel behavior arising from the antiroton effect, notably a rapid rising and upwardly curving shape. These features make identifying the speed of sound difficult from a visual inspection of the results. Furthermore, in the previous subsections we noted that the lowest band can be dynamically unstable at very low k_z, which corresponds to c_z being imaginary (i.e., $Mc_z^2 < 0$).

The variational spectrum in Eq. (14) neglects any change in the transverse profile for long wavelength excitations and thus does not provide a good estimate of the speed of sound. So for the variational approach it is better to use the result $Mc_z^2 = n(\partial n / \partial \mu)$ for the inverse (axial) compressibility:[6]

$$Mc_{\text{var}}^2 = n \left(\frac{\partial^2 \mathcal{E}}{\partial n^2} \right), \tag{19}$$

$$= n\tilde{U}_0(0) \left(1 - \frac{n}{l} \frac{dl}{dn} \right) + \frac{3n^{3/2} \gamma_{\text{QF}} \gamma_\chi}{2} \left(1 - \frac{6}{5} \frac{n}{l} \frac{dl}{dn} \right), \tag{20}$$

---

[6]Note we can also use this result to obtain Mc_z^2 directly from the EGPE rather than calculating the BdG excitations. We have verified that the results are identical from these two approaches.
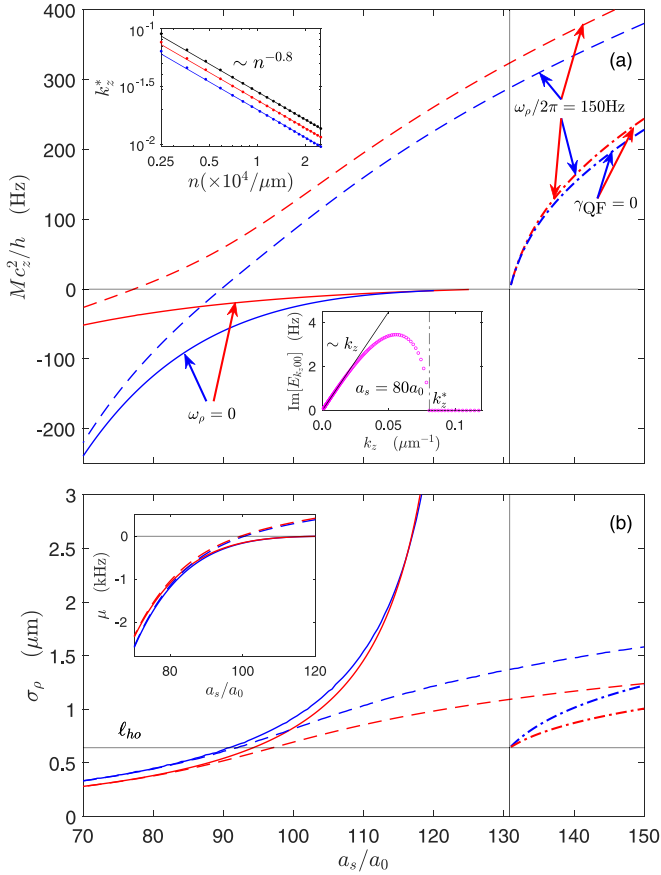
FIG. 6. (a) Mc_z^2 [16] as a function of a_s for fixed linear density $n = 2.5 \times 10^3/\mu m$ from EGPE (blue lines) and variation (red line) calculations. Results are shown for infinite free-space droplets (solid line), transversally confined infinite droplets (dashed line) and a transversally confined condensate with $\gamma_{QF} = 0$ (dashed-dotted line). The upper inset shows how k_z^* varies with n for $a_s/a_0 = 75$ (black line, top), 80 (red line, middle), and 85 (blue line, bottom). The lower inset shows the imaginary part of the E_{k_z00} spectrum for a free-space droplet with $a_s = 80a_0$. (b) The radial $1/e$-density widths of the states. These results use $a_{dd} = 130.8a_0$, and for trapped cases $\omega_\rho/2\pi = 150$ Hz is used.

where $\tilde{U}_0(0) = (g_s - g_{dd})/2\pi l^2$ [from Eq. (15)], and

$$\frac{n}{l}\frac{dl}{dn} = \frac{n\tilde{U}_0(0) + \frac{9}{5}n^{3/2}\gamma_{QF}\gamma_\chi}{\frac{3\hbar^2}{ml^2} + \frac{ml^2\omega_\rho^2}{2} + 3n\tilde{U}_0(0) + \frac{24}{5}n^{3/2}\gamma_{QF}\gamma_\chi}. \quad (21)$$

In Fig. 6(a) we plot Mc_z^2 as a function of a_s for infinite droplets in free-space and with transverse confinement. For reference, we also show the behavior of a transversally confined system without quantum fluctuations, where $Mc_z^2 \to 0$ (and the system collapses) as $a_s \to a_{dd}$ from above. Comparing the trapped results we observe that inclusion of quantum fluctuations causes a significant increase in Mc_z^2. However, even including quantum fluctuation effects Mc_z^2 becomes negative for sufficiently low values of a_s (i.e., $a_s \lesssim 90a_0$). For the infinite free-space droplet at all values of a_s where a localized droplet state is obtained, we find that $Mc_z^2 < 0$.

A negative value of Mc_z^2, i.e., when c_z is imaginary, indicates that the long wavelength modes of the system are

dynamically unstable. The lower inset to Fig. 6(a) shows the imaginary part of the spectrum for an infinite free-space droplet with $a_s = 80a_0$. Here the E_{k_z00} excitation band is purely imaginary for $k_z < k_z^*$ and real thereafter. For the finite-sized droplet the longest wavelength excitation has a wave vector of approximately $k_{z,\min} \equiv \pi/\sigma_z$ (cf. the first $m = 0$ excitation marked by a symbol in Fig. 5), where σ_z is the $1/e$-density half-width introduced earlier. Thus the finite axial extent of the droplet prevents the unstable modes being accessed, and so the dynamical instability cannot manifest. The upper inset to Fig. 6(a) shows results for how the maximum unstable wave vector k_z^* changes with a_s and n. For larger finite droplets, where n is higher, k_z^* gets smaller, possibly indicating that the instability cannot manifest even in very large droplets. This is consistent with the observations in Ref. [21] where the lowest energy $m = 0$ mode of a finite droplet appears to asymptotically approach 0 as N increases.

The width σ_ρ of the infinite free-space droplet diverges with increasing a_s [see Fig. 6(b)], as the droplet unbinds and evaporates. Using the variational theory we can solve for the evaporation transition, i.e., where a stationary state solution (i.e., $d\mathcal{E}/dl = 0$) occurs with $\mathcal{E} = 0$, giving

$$\frac{1}{2} + n(a_s - a_{dd}) = 0. \quad (22)$$

For the free-space droplet case in Fig. 6 this result predicts evaporation to occur at $a_s = 127a_0$. Because the radial width diverges as we approach the transition we have not been able to numerically explore the infinite droplet EGPE predictions for the transition in detail. For a finite droplet, as σ_ρ increases the infinite droplet becomes a poor approximation, since it requires $\sigma_z \gg \sigma_\rho$. Thus, condition (22) is not a useful predictor of the transition in a finite droplet.

D. Thermodynamic limit droplet of a free-space droplet

Finally we consider the thermodynamic limit of a free-space dipolar droplet. We take the thermodynamic limit by allowing N to increase towards infinity in a finite free-space droplet. We find (e.g., from fits in Fig. 4(c)–4(e), also see Ref. [21]) that the following approximately scaling behavior holds:

$$\sigma_\rho \sim N^{1/4}, \quad (23)$$

$$\sigma_z \sim N^{1/2}, \quad (24)$$

$$n \sim \sigma_\rho^2 \sim N^{1/2}, \quad (25)$$

for the width, length, and linear density of the droplet, respectively. Thus, in the thermodynamic limit all of these quantities are infinite. Hence, the thermodynamic limit does not correspond to the infinite droplet theory developed in this paper, in which σ_z is infinite, but σ_ρ and n are both finite.

IV. CONCLUSIONS AND OUTLOOK

In this paper we have developed a theory to describe an infinitely long dipolar droplet, as an idealization of the long-filament-shaped droplets prepared in experiments. Our focus has been on the excitation properties, which are difficult to calculate accurately for finite droplets. Our results in Fig. 5

demonstrate good quantitative agreement to one of the few detailed studies of excitations of a finite dipolar droplet in the literature. In the excitation spectrum, a number of interesting features arise, collectively called the antiroton effect [16]. These features appear in our results for the dynamic structure factor of an infinite droplet, which could be measured in experiments by performing Bragg spectroscopy along the long axis of a large droplet.

We have also examined the nature of the axial speed of sound in a droplet. For the infinite droplet theory we find that $Mc_z^2 < 0$ for free-space droplets and in confined droplets with sufficiently low values of a_s. The $k_z \to 0$ limit used to identify the speed of sound is problematic for finite droplets due to prominent finite-size dependence arising from the antiroton effect (i.e., the rapid change in the effective interaction with k_z near $k_z = 0$). Indeed, finite dipolar droplets appear to be stable because the unstable modes occur at wavelengths that are too long to be accommodated. Increasing N to make the droplet longer also causes n to increase (the droplet gets wider), and our results show that this leads to unstable wavelengths becoming even longer. Thus, it is possible that these instabilities never manifest in finite droplets, and certainly this is consistent with calculations we have performed for finite droplets over a wide parameter regime. This also raises the question: what is the appropriate axial speed of sound for a finite droplet? In practice a result reflecting the finite size of the system may be necessary, e.g., replacing $k_z = 0$ with $k_z \to 1/\sigma_z$ in Eq. (18). Whether such an identification is useful in understanding the effective compressibility or critical velocity of a finite droplet is an interesting direction for future research.

[1] H. Kadau, M. Schmitt, M. Wenzel, C. Wink, T. Maier, I. Ferrier-Barbut, and T. Pfau, Observing the Rosensweig instability of a quantum ferrofluid, Nature (London) **530**, 194 (2016).

[2] I. Ferrier-Barbut, H. Kadau, M. Schmitt, M. Wenzel, and T. Pfau, Observation of Quantum Droplets in a Strongly Dipolar Bose Gas, Phys. Rev. Lett. **116**, 215301 (2016).

[3] M. Schmitt, M. Wenzel, F. Böttcher, I. Ferrier-Barbut, and T. Pfau, Self-bound droplets of a dilute magnetic quantum liquid, Nature (London) **539**, 259 (2016).

[4] L. Chomaz, S. Baier, D. Petter, M. J. Mark, F. Wächtler, L. Santos, and F. Ferlaino, Quantum-Fluctuation-Driven Crossover from a Dilute Bose-Einstein Condensate to a Macro-droplet in a Dipolar Quantum Fluid, Phys. Rev. X **6**, 041039 (2016).

[5] C. R. Cabrera, L. Tanzi, J. Sanz, B. Naylor, P. Thomas, P. Cheiney, and L. Tarruell, Quantum liquid droplets in a mixture of Bose-Einstein condensates, Science **359**, 301 (2018).

[6] K. E. Wilson, N. Westerberg, M. Valiente, C. W. Duncan, E. M. Wright, P. Öhberg, and D. Faccio, Observation of Photon Droplets and Their Dynamics, Phys. Rev. Lett. **121**, 133903 (2018).

[7] D. Baillie, R. M. Wilson, R. N. Bisset, and P. B. Blakie, Self-bound dipolar droplet: A localized matter wave in free space, Phys. Rev. A **94**, 021602(R) (2016).

[8] F. Wächtler and L. Santos, Ground-state properties and elementary excitations of quantum droplets in dipolar Bose-Einstein condensates, Phys. Rev. A **94**, 043618 (2016).

[9] T. D. Lee, K. Huang, and C. N. Yang, Eigenvalues and eigenfunctions of a Bose system of hard spheres and its low-temperature properties, Phys. Rev. **106**, 1135 (1957).

[10] A. R. P. Lima and A. Pelster, Quantum fluctuations in dipolar Bose gases, Phys. Rev. A **84**, 041604(R) (2011).

[11] A. R. P. Lima and A. Pelster, Beyond mean-field low-lying excitations of dipolar Bose gases, Phys. Rev. A **86**, 063609 (2012).

[12] D. S. Petrov, Quantum Mechanical Stabilization of a Collapsing Bose-Bose Mixture, Phys. Rev. Lett. **115**, 155302 (2015).

[13] H. Saito, Path-integral Monte Carlo study on a droplet of a dipolar Bose-Einstein condensate stabilized by quantum fluctuation, J. Phys. Soc. Jpn. **85**, 053001 (2016).

[14] F. Wächtler and L. Santos, Quantum filaments in dipolar Bose-Einstein condensates, Phys. Rev. A **93**, 061603(R) (2016).

[15] R. N. Bisset, R. M. Wilson, D. Baillie, and P. B. Blakie, Ground-state phase diagram of a dipolar condensate with quantum fluctuations, Phys. Rev. A **94**, 033619 (2016).

[16] S. Pal, D. Baillie, and P. B. Blakie, Excitations and number fluctuations in an elongated dipolar Bose-Einstein condensate, Phys. Rev. A **102**, 043306 (2020).

[17] F. Böttcher, M. Wenzel, J.-N. Schmidt, M. Guo, T. Langen, I. Ferrier-Barbut, T. Pfau, R. Bombín, J. Sánchez-Baena, J. Boronat, and F. Mazzanti, Dilute dipolar quantum droplets beyond the extended Gross-Pitaevskii equation, Phys. Rev. Research **1**, 033088 (2019).

[18] E. J. Halperin and J. L. Bohn, Hyperspherical approach to dipolar droplets beyond the mean-field limit, Phys. Rev. A **104**, 033324 (2021).

[19] M. Edmonds, T. Bland, and N. Parker, Quantum droplets of quasi-one-dimensional dipolar Bose–Einstein condensates, J. Phys. Commun. **4**, 125008 (2020).

[20] T. Lahaye, C. Menotti, L. Santos, M. Lewenstein, and T. Pfau, The physics of dipolar bosonic quantum gases, Rep. Prog. Phys. **72**, 126401 (2009).

[21] D. Baillie, R. M. Wilson, and P. B. Blakie, Collective Excitations of Self-Bound Droplets of a Dipolar Quantum Fluid, Phys. Rev. Lett. **119**, 255302 (2017).

[22] S. Ronen, D. C. E. Bortolotti, and J. L. Bohn, Radial and Angular Rotons in Trapped Dipolar Gases, Phys. Rev. Lett. **98**, 030406 (2007).

[23] H.-Y. Lu, H. Lu, J.-N. Zhang, R.-Z. Qiu, H. Pu, and S. Yi, Spatial density oscillations in trapped dipolar condensates, Phys. Rev. A **82**, 023622 (2010).

[24] A.-C. Lee, D. Baillie, and P. B. Blakie, Numerical calculation of dipolar-quantum-droplet stationary states, Phys. Rev. Research **3**, 013283 (2021).

[25] S. Giovanazzi and D. H. J. O'Dell, Instabilities and the roton spectrum of a quasi-1D Bose-Einstein condensed gas with dipole-dipole interactions, Eur. Phys. J. D **31**, 439 (2004).

[26] J. Stenger, S. Inouye, A. P. Chikkatur, D. M. Stamper-Kurn, D. E. Pritchard, and W. Ketterle, Bragg Spectroscopy of a Bose-Einstein Condensate, Phys. Rev. Lett. **82**, 4569 (1999).

[27] D. M. Stamper-Kurn, A. P. Chikkatur, A. Görlitz, S. Inouye, S. Gupta, D. E. Pritchard, and W. Ketterle, Excitation of Phonons in a Bose-Einstein Condensate by Light Scattering, Phys. Rev. Lett. **83**, 2876 (1999).

[28] P. B. Blakie, R. J. Ballagh, and C. W. Gardiner, Theory of coherent Bragg spectroscopy of a trapped Bose-Einstein condensate, Phys. Rev. A **65**, 033602 (2002).

[29] D. Petter, G. Natale, R. M. W. van Bijnen, A. Patscheider, M. J. Mark, L. Chomaz, and F. Ferlaino, Probing the Roton Excitation Spectrum of a Stable Dipolar Bose Gas, Phys. Rev. Lett. **122**, 183401 (2019).

[30] D. Petter, A. Patscheider, G. Natale, M. J. Mark, M. A. Baranov, R. van Bijnen, S. M. Roccuzzo, A. Recati, B. Blakie, D. Baillie, L. Chomaz, and F. Ferlaino, Bragg scattering of an ultracold dipolar gas across the phase transition from Bose-Einstein condensate to supersolid in the free-particle regime, Phys. Rev. A **104**, L011302 (2021).

[31] R. M. Wilson, S. Ronen, and J. L. Bohn, Critical Superfluid Velocity in a Trapped Dipolar Gas, Phys. Rev. Lett. **104**, 094501 (2010).

[32] C. Ticknor, R. M. Wilson, and J. L. Bohn, Anisotropic Superfluidity in a Dipolar Bose Gas, Phys. Rev. Lett. **106**, 065301 (2011).

[33] G. Bismut, B. Laburthe-Tolra, E. Maréchal, P. Pedri, O. Gorceix, and L. Vernac, Anisotropic Excitation Spectrum of a Dipolar Quantum Bose Gas, Phys. Rev. Lett. **109**, 155302 (2012).

[34] D. Baillie, R. N. Bisset, C. Ticknor, and P. B. Blakie, Number Fluctuations of a Dipolar Condensate: Anisotropy and Slow Approach to the Thermodynamic Regime, Phys. Rev. Lett. **113**, 265301 (2014).

[35] M. Wenzel, F. Böttcher, J.-N. Schmidt, M. Eisenmann, T. Langen, T. Pfau, and I. Ferrier-Barbut, Anisotropic Superfluid Behavior of a Dipolar Bose-Einstein Condensate, Phys. Rev. Lett. **121**, 030401 (2018).